ACS Catalysis

Research Article

pubs.acs.org/acscatalysis

Supported Iron Fischer–Tropsch Catalyst: Superior Activity and Stability Using a Thermally Stable Silica-Doped Alumina Support

Kamyar Keyvanloo,[†] Maryam Khosravi Mardkhe,[‡] Todd M. Alam,[§] Calvin H. Bartholomew,[†] Brian F. Woodfield,[‡] and William C. Hecker*[,†]

[†]Department of Chemical Engineering, [‡]Department of Chemistry and Biochemistry, Brigham Young University, Provo, Utah 84602
[§]Department of Electronic, Optical and Nanostructured Materials, Sandia National Laboratories, Albuquerque, NM, 87185

Supporting Information

ABSTRACT: Fischer–Tropsch synthesis (FTS) is a technically proven and economically viable route for the conversion of coal, biomass, and natural gas to hydrocarbon fuels. Although *unsupported* Fe catalysts are proven for FTS, they lack the physical strength and durability that would make them more viable for large-scale commercial reactors, and their activity is still significantly less than that of Co FT catalysts. In this work, we report on a very active and stable *supported* Fe FT catalyst that is more active than any *supported* Fe FT catalyst previously reported and competitive with the best *unsupported* catalysts. In addition, its productivity, which takes into account selectivity to desired hydrocarbon products, is also very competitive. More importantly, the catalyst is extremely stable, as evidenced by the fact that after 700 h on stream, its activity and productivity are still increasing. These catalyst properties result from using a novel γ-alumina support material doped with silica and pretreated at 1100 °C. This unique support has high pore volume, large pore diameter, and unusually high thermal stability. The ability to pretreat this support at 1100 °C enables preparation of a material having a low number of acid sites and weak metal oxide–support interactions, all desirable properties for an FT catalyst. These results demonstrate that the surface chemistry of the support material plays a crucial role in the design of an active and stable supported Fe FT catalyst.

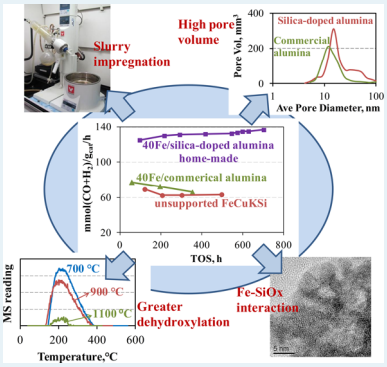

KEYWORDS: *Fischer–Tropsch, supported iron catalyst, silica-doped alumina, stable, active*

INTRODUCTION

Fischer–Tropsch synthesis (FTS) is a commercially proven, economically viable, and environmentally sound process for the production of hydrocarbon fuels from low-value natural gas, coal, and biomass. Nevertheless, improvements in catalyst technology are desirable to improve the efficiency and economics of this process. Iron catalysts are considered to be more favorable than cobalt catalysts for the production of long-chain hydrocarbons from coal or biomass using low temperature FT conditions (LTFT) because of their low cost, low methane selectivity, and high water-gas shift (WGS) activity; WGS activity is needed for internal production of H_2 during FTS because of the inherently low H_2/CO ratios of syngas produced from coal or biomass.

Typical commercial iron LTFT catalysts consist of unsupported iron promoted with copper and potassium and texturized with silicon oxide. Several publications from Bukur et al.[1] describe development of active, selective, and stable precipitated iron catalysts (unsupported), including one containing 3 Cu/4 K/16 SiO_2 per 100 parts Fe with a weight–time yield of 450 mmol $(CO + H_2)/g_{Fe}/h/MPa$ at 260 °C and 2.2 MPa. This activity is among the highest reported for iron catalysts. Unfortunately, despite favorable high activity and selectivity properties, these unsupported iron catalysts are generally weak mechanically, which can lead to high rates of attrition during their use in slurry bubble column reactors (SBCRs). Catalyst attrition causes formation of 1–10 μm diameter particles that are very difficult to separate from product wax in SBCRs. The use of binder materials in the catalyst can decrease the attrition problems somewhat, but may also decrease catalyst activity. Nevertheless, commercial entities have developed attrition-resistant, unsupported Fe FT SBCR catalysts for 5 m SBCRs through the generous use of binders;[3] however, these catalysts still suffer attrition due to the higher gas velocities in 10 m SBCRs. Moreover, if sufficient binder is incorporated, the composition of the "unsupported catalyst" approaches that of a supported catalyst of high metal loading.

Thus, in principle, an alumina-supported iron catalyst is likely to be stronger and more attrition-resistant than an unsupported Fe catalyst incorporating binders.[4] Unfortunately, in practice, previous attempts to develop supported iron FT catalysts have met with limited success because most of these catalysts were found to have low activity and high methane selectivity.[2,4,6] For example, Bukur et al.[1d,2] reported an Fe catalyst supported on SiO_2 to be nearly 3-fold less active than their most active unsupported catalyst (100 vs 269 mmol $(CO + H_2)/g_{cat}/MPa/h$), and their alumina-supported catalyst was even less active

Received: December 26, 2013
Revised: February 6, 2014
Published: February 11, 2014

   dx.doi.org/10.1021/cs401242d | ACS Catal. 2014, 4, 1071–1077

(~60 mmol $(CO + H_2)/g_{cat}/MPa/h$). The Davis group[4,5] found a similar result. Their most active alumina-supported Fe catalyst was still 5-fold less productive than unsupported iron (0.09 vs 0.45 $g_{HC}/g_{cat}/h$) and had high methane selectivity. The poor performance of these catalysts can be attributed to less than ideal preparation methods, support materials favoring strong Fe oxide−support interactions and attendant low reducibility to active Fe carbides, decoration of the active carbide phase by support moieties,[2,7] or some combination of the above.

To overcome these problems, Xu and Bartholomew[6] prepared 10% Fe/silica and FePt/silica catalysts via nonaqueous evaporative impregnation of a previously dehydroxylated silica support (at 600 °C). The properties of their catalysts included relatively high extents of reduction following reduction at 300 °C in H_2, moderate dispersions (5−16%), a productivity for 10% $FePtK/SiO_2$ of 0.30 $g_{HC}/g_{cat}/h$ and methane selectivities of 8−10 mol %. Nevertheless, their reported activity was still nearly 4-fold lower than Bukur's best unsupported catalyst (62 vs 269 mmol $(CO + H_2)/g_{cat}/MPa/h$). Although this was due partly to the low Fe loading, it was still in the range of the previous low-activity supported catalysts.[2,4]

The use of weakly interacting α-alumina and carbon nanofiber supports to decrease the interaction between iron and the support for high temperature FT reactions to produce olefins was recently reported in *Science* and *JACS*;[8] however, these high temperature (HT) catalysts have low metal loadings and would not have sufficient activity for LTFT. High iron loadings with their attendant high active site densities are needed for high productivity,[2] and it is not feasible to have high loadings on low-surface-area α-alumina. Carbon nanotubes (CNTs) have also been used as a support in FTS[9] and show easier reduction and carbiding due to their inert surface chemistry, but they are prohibitively expensive for use in commercial FTS plants.

Therefore, using a support with high surface area and high thermal stability, which enables its dehydroxylation at high temperatures, should be important in FTS. A weakly interacting γ-alumina support rather than α-alumina should also provide more pore volume and surface area for high iron loading and easier carbiding of Fe nanoparticles. The greater degree of dehydroxylation should retard the formation of $FeO.Al_2O_3$, and all of these properties should result in higher activity. In addition, the alumina support will provide higher attrition resistance and crush strength compared with unsupported Fe catalyst and could lead to improved catalysts for large fixed-bed and SBCRs.

In this paper, we report, for the first time, the successful preparation of a very active and stable supported Fe LTFT catalyst, that is, an Fe/Cu/K catalyst on a silica-doped γ-alumina (AlSi) support material of high thermal stability but having weak interactions with Fe oxide. Key factors leading to the excellent performance of this catalyst were (1) the use of nonaqueous, wet impregnation in a rotary evaporator; (2) utilization of a new silica-stabilized alumina support (AlSi) with very high pore volume and large pores; (3) high temperature pretreatment of the AlSi support to give a minimal concentration of surface OH groups, which are known to interact strongly with Fe oxide; and (4) stabilization of Fe phases against sintering due to the presence of silica on the support surface. We also prepared an Fe/Cu/K catalyst on a conventional γ-alumina support (AlG) and an unsupported FeCuKSi for comparison.

EXPERIMENTAL METHODS

Preparation of Silica-Doped Alumina Support (AlSi). The silica-doped alumina support (AlSi) was prepared using a "one-pot" solvent-deficient method starting with aluminum isopropoxide ($C_9H_{21}O_3Al$) (granular, 98+%) (AIP) and tetraethyl orthosilicate ($SiC_8H_{20}O_4$) (liquid, 99.9%) (TEOS), both purchased from Alfa-Aeser. Specifically, water was added to AIP in a 5:1 molar ratio and mixed briefly. TEOS was then added with a small amount of additional water (1:2 molar ratio) in a quantity sufficient to give 5 wt % silica in the final support material. The resulting mixture was then stirred for 30 min in a Bosch mixer, followed by thermal treatment at 700 °C in air for 2 h with a heating rate of approximately 2.5 °C/min to form γ-alumina. The product was then cooled to room temperature, after which it was heated to 1100 °C over 5 h and held at 1100 °C for 2 h.[10]

Preparation of 40Fe/AlSi and 40Fe/AlG Catalysts. Just as 5% silica was added to the AlSi support material to improve its properties, including thermal stability, likewise, 3 wt % La was added to the St. Gobein alumina (AlG) (as described previously[11]) in preparing the 40 Fe/AlG catalyst. Following addition of the La, the material was sieved to 30−60 mesh and then calcined at 700 °C in air for 4 h. 40Fe/AlSi and 40Fe/AlG catalysts were then prepared by coimpregnation of the given support with a nonaqueous solution (50% iso-propanol and 50% acetone) containing the desired amounts of ferric nitrate and copper nitrate in multiple steps. In each step, 10 wt % Fe with the desired amount of Cu was dissolved in a volume of solution corresponding to 10% above incipient wetness and then was placed in a rotary evaporator and mixed for 12 h to give a uniform Fe deposition. The catalysts were then dried slowly in vacuum at 50 °C for 12 h followed by 80 °C in air overnight. After drying, the samples were calcined at 300 °C for 16 h in air. Potassium bicarbonate was then added by incipient-wetness aqueous impregnation, followed by additional drying and impregnation steps. Nominal compositions (on a relative mass basis) of synthesized catalysts were 100 Fe/7.5 Cu/4 K/150 Al_2O_3.

Preparation of Unsupported Fe Catalyst. Solvent-deficient precipitation (SDP) produces metal oxide nanomaterials[10a,12] that can be used as supports, oxide catalysts, or catalyst precursors. Unsupported Fe catalyst was prepared by coprecipitation of iron nitrate, copper nitrate, potassium bicarbonate, and silica with ammonium bicarbonate in a solvent deficient environment. After precipitation, it was dried at 120 °C overnight and calcined at 300 °C for 16 h. The resulting oxide precursors are denoted throughout as FeCuKSi.

Catalyst Characterizations. Powder X-ray diffraction (XRD) measurements were carried out using a Panalytical X'Pert Pro X-ray diffractometer with Cu Kα radiation (λ =0.15418 nm) at a scanning rate of 0.02° s^{-1} in the range from 10° to 90° in 2θ. The XRD power source was (40 kV, 40 mA).

Nitrogen adsorption measurements were done using a Micromeritics Tristar 3020 for the determination of surface properties at −196 °C. Samples were degassed at 200 °C under N_2 flow overnight before each measurement. Average pore diameter and pore size distribution were calculated for each support and catalyst using a new slab pore model and method proposed by Huang and Bartholomew[14] and modified to fit a log-normal PSD.[15]

NMR spectra were obtained on a Bruker Avance I 400 (9.6 T) NMR instrument using a 7 mm (^{29}Si) or a 4 mm (^{27}Al) broadband MAS Probe. All spectra were obtained at room temperature, and a spinning speed of 12.5 kHz for ^{27}Al and 4 kHz for ^{29}Si. The 1D ^{29}Si MAS NMR spectra were obtained using a single pulse Block decay using a 240 s recycle delay, and the $^{1}H-^{29}Si$ CPMAS spectra was obtained using a 5 ms contact time.

dx.doi.org/10.1021/cs401242d | ACS Catal. 2014, 4, 1071−1077

The ^{27}Al MAS spectra were obtained using a single pulse Bloch decay. The ^{27}Al chemical shift was referenced to 1 M $Al(H_2O)_{6+}$ in water δ = 0.0 ppm, and the ^{29}Si was referenced to Q_8M_8 δ = +12.6 ppm with respect to TMS (δ = 0 ppm). Spectral simulations were performed using DMFIT.[16]

X-ray photoelectron spectroscopy (XPS) was performed using a SSX-100 ESCA spectrometer equipped with a monochromatic Al Kα source (1486.6 eV) and a hemispherical analyzer. A small amount of prepared nanoparticle sample was pressed on ~1.5 × 1.5 cm^2 indium (99.99%) foil for XPS analysis. All XPS spectra were referenced to the In 3d peak at 451 eV. A flood gun was not required during the analysis. [Note: Before using indium foil, other sample preparation methods were tried in which a thin layer of nanoparticle sample was pressed onto a double-sided sticky tape (conductive carbon tape, kapton tape, and scotch tape) or the nanaparticle sample was pressed to form a pellet. The XPS spectra of such prepared samples showed undesired peak splitting due to sample charging, which could not be reliably corrected by using a flood gun. In comparison, with the indium foil method, no flood gun was needed.]

Syngas temperature-programmed-reduction (syngas-TPR) experiments were performed in a Mettler Toledo TGA/DSC 1 equipped with an automated GC 200 gas controller to determine reduction and carbiding behavior of the supported catalysts; 10–20 mg of calcined samples were exposed to 10% syngas (H_2:CO = 1) in He while the temperature was increased at 3 °C/min from ambient to 700 °C.

Ammonia-TPD experiments were performed on AlSi to determine total acid sites. A sample of 100 mg was degassed in situ at 550 °C for 1 h under helium flow of 30 sccm. The sample was cooled to an adsorption temperature of 100 °C. After 1 h of NH_3 adsorption, it was switched to He to remove any physisorbed ammonia. The sample was then heated in 10 sccm He flow with a ramp rate of 5 °C/min to 500 °C. The effluent gas concentrations were determined using a Pfeiffer Vacuum ThermoStar mass spectrometer.

Fixed-Bed Catalyst Activity Tests. Fischer–Tropsch Synthesis was conducted in a fixed-bed reactor (stainless steel, 3/8 in. OD) described previously.[17] Each sample (0.25 g, 250–590 μm) was diluted with silicon carbide to improve temperature stability in the catalytic zone. Before FTS, the samples were reduced in situ at 280–320 °C in 10% H_2/He for 10 h, followed by 100% H_2 for 6 h. Then the catalysts were cooled to 180 °C. The system was then pressurized to 2.1 MPa in syngas (H_2/CO = 1), and the catalysts were activated at 280 °C for 48–90 h. Reaction temperatures were varied from 220 to 260 °C and the H_2/CO ratio was varied from 0.66 to 1.0. (In addition to CO and H_2, the feed gas contained 20–40% helium used as a diluent to keep the total pressure the same for all runs.) The exit gas and liquid effluent passed through a hot trap (90 °C) and a cold trap (0 °C) to collect heavy hydrocarbons and liquid products. The effluent gaseous product was analyzed using an HP5890 gas chromatograph equipped with a thermal conductivity detector and 60/80 carboxene-1000 column. Carbon monoxide conversions and selectivities were determined with the aid of an Ar tracer.

RESULTS

After the AlSi support material was prepared, it was calcined at 1100 °C for 2 h, a temperature much higher than that used to calcine typical γ-aluminas. Surprisingly, both the pore volume (1.06 cm^3/g) and average pore diameters of the calcined AlSi support remain unusually large for a γ-alumina following such a severe treatment. The pore size distribution is bimodal, with a relatively sharp peak at ~20 nm and a very broad peak from ~30 to 55 nm (see Figure 1). By contrast, the pore volume and average pore diameter of a commercial (Sasol) silica-doped alumina are 0.50 cm^3/g and 8.3 nm (Table S1, Supporting Information).[18]

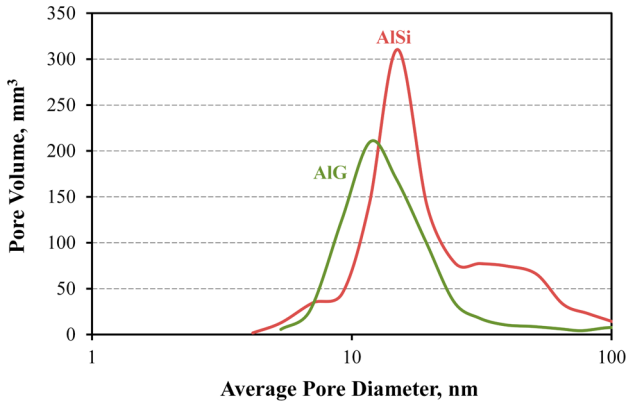

Figure 1. Pore size distribution of silica-doped alumina (AlSi) calcined at 1100 °C and St. Gobein alumina (AlG) calcined at 700 °C.

The pore volume for 40Fe/AlSi of 0.64 cm^3/g even with 40% iron loading was quite high; it is 30% higher than that of 40Fe/AlG and is a factor of 6 higher than that for the unsupported catalyst (FeCuKSi, Table 1).

Table 1. Surface Area, Total Pore Volume, and Average Pore Diameters of Two Support Materials and Three Calcined Catalysts of This Study

			av pore diam (nm)	
sample	BET surface area (m^2/g)	pore vol (cm^3/g)	1st peak	2nd peak
AlSi–support	184	1.06	22.5	52
40Fe/AlSi	173	0.64	21.8	29
AlG–support	216	0.65	18.1	
40Fe/AlG	152	0.46	16.4	
FeCuKSi	105	0.11	6.8	

Average crystallite diameters (d_{cryst}) for the reduced and carbided catalysts were calculated from X-ray diffraction (XRD) measurements (Figure S1, Supporting Information (SI)) using the Scherrer formula and are shown in Table S2 (SI). The catalysts were passivated after reduction or carbiding. The carbided forms of both 40Fe/AlSi and 40Fe/AlG show the presence of Fe_5C_2, and both have d_{cryst} values of ~8 nm. Fe_5C_2 is considered by many researchers[2,6,8,19] to be the active phase for Fe FTS.

The three catalysts of this study were tested in a fixed-bed reactor at 250 °C, 2.1 MPa, and H_2/CO = 1, which are typical operating conditions for Fe FTS. Data in SI Table S3 show that the initial activity for 40Fe/AlSi is 42% and 67% higher than that for 40Fe/AlG and unsupported FeCuKSi, respectively. Figure 2 shows changes in activity (mmol (CO + H_2)/g_{cat}/h at 250 °C) with time on stream (TOS) up to 700 h. The activity of 40Fe/AlG decayed with time; after 350 h, it was essentially the same as for the unsupported catalyst. On the other hand, the activity for Fe/AlSi is observed to increase with TOS, even up to 700 h when the run was terminated; at this point, the catalyst activity was 13%

dx.doi.org/10.1021/cs401242d | ACS Catal. 2014, 4, 1071–1077

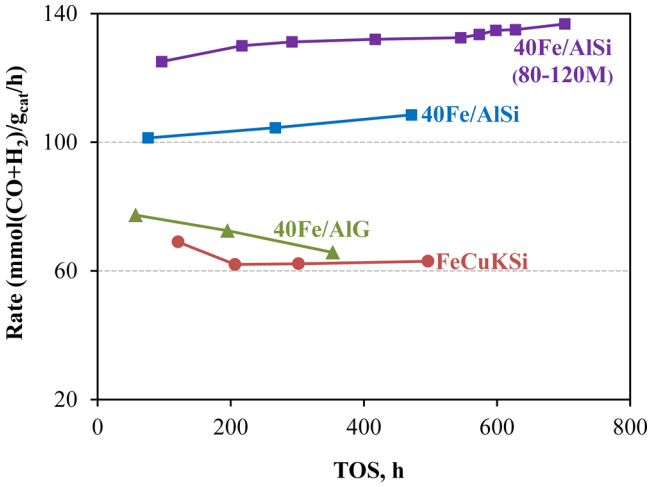

Figure 2. Catalyst activity with TOS at 250 °C, H_2/CO:1, 2.2 MPa for three catalysts of 30−60 mesh size and a second sample of 40Fe/AlSi with an 80−120 mesh size.

higher than its initial value. Two sets of data for 40Fe/AlSi appear in Figure 2. Initially, a catalyst particle size of ∼430 μm (30−60 mesh) was used for all 3 catalysts; later, the most active catalyst (40Fe/AlSi) was also tested using a smaller particle size of ∼150 μm (80−120 mesh) for which the activity was found to be 30% higher. This was probably due to a small pore diffusional influence on the 430 μm catalyst.

Figure 3 and Tables S4 and S5 (SI) compare the performance of the 40Fe/AlSi (150 μm) catalyst with results reported previously for supported and unsupported Fe catalysts. Apparent first-order reaction rate constants (k_{cat}, k_{Fe}) were calculated to correct for differences in hydrogen partial pressure.[2] The data indicate that the k_{cat} (rate constant per gram of catalyst) at 260 °C for 40Fe/AlSi is 3.5 times higher than the k_{cat} for the Fe/silica catalyst of Bukur et al. and 7 times higher than that for their Fe/alumina catalyst. Moreover, the k_{cat} for 40Fe/AlSi is nearly 30% higher than that of the most active *unsupported* catalyst of Bukur et al.;[1d] that is, 325 versus 269 mmol $(H_2 + CO)/g_{cat}$/ MPa/h. On a per gram Fe basis, the k_{Fe} for 40Fe/AlSi is twice as high: 878 vs 450 mmol $(H_2 + CO)/g_{Fe}$/MPa/h. It should be acknowledged here that the selectivities of the 40Fe/AlSi are less favorable than those for Bukur et al. (see SI Table S4), i.e., the C_{3+} selectivity on a CO_2-free basis of the 40Fe/AlSi is slightly lower (83 vs 90%) and $C_1 + C_2$ selectivity is higher (12.4 vs 6.3%) than that of Bukur's unsupported catalyst. Nevertheless, catalyst productivity (which takes into account both activity and selectivity) is 40% higher for 40Fe/AlSi than Bukur's unsupported catalyst on a per mass of iron basis (g_{HC}/g_{Fe}/h), whereas the productivities based on mass of catalyst are essentially the same, as seen in Figure 3B. Recently, Davis's group reported preparation of a very active unsupported Fe catalyst with productivity of 0.73 g_{HC}/g_{cat}/h.[20]

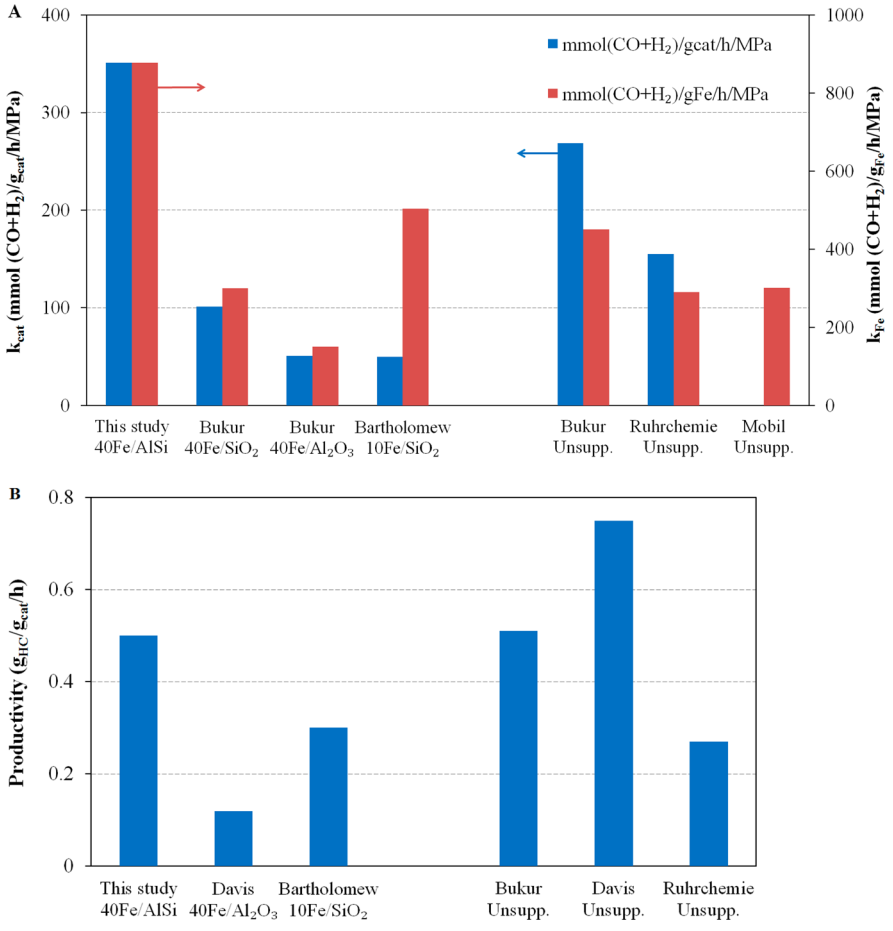

Figure 3. Comparison of (A) first-order rate constants, and (B) productivities (g_{HC}/g_{cat}/h) for various supported and unsupported iron catalysts at 260 °C. The left axis in part A represents the rate constant per gram of catalyst (blue), and the right axis is the rate constant per gram of Fe (red). (More details are shown in Tables S4 and S5 (SI).)

dx.doi.org/10.1021/cs401242d | *ACS Catal.* 2014, 4, 1071−1077

Activity and productivity comparisons are also made to other unsupported and supported catalysts in Figure 3 and Table S5 (SI), including comparisons with industrial catalysts from Ruhrchemie[21] and Mobile[22] as well as academic catalysts from U.C. Berkeley[23] and U. Kentucky.[4,20]

Previous to this work, it was supposed that unsupported Fe catalysts were significantly more active for FTS than supported Fe catalysts, since no supported catalyst had approached the activity of the unsupported catalysts. However, the results of the current study clearly show that by all measures of activity, 40Fe/AlSi is more active (by 2−7 times) and productive than any other supported Fe FT catalyst previously reported and that it is competitive with unsupported Fe FT catalysts previously reported. Moreover, this catalyst is also extremely stable, at least up to a TOS of 700 h, as its activity actually increased over that time period.

DISCUSSION

Four keys to the outstanding performance of our iron catalyst supported on silica-doped alumina (40Fe/AlSi) were introduced earlier and are addressed and justified in more detail below.

1. Nonaqueous, wet-impregnation using rotary-evaporator. The use of a wet, rotated, slurry impregnation with vacuum drying of the nonaqueous solution provides a homogeneous distribution of iron nanoparticles on the support[6,23,24] which results in small (8 nm) crystallites in both 40Fe/AlSi and 40Fe/AlG (see Table S2, SI). These are much smaller than the typical diameters of 25−30 nm observed for commercial Fe catalysts.

2. High pore volume and large pore diameters in the AlSi support facilitate (1) a spatially uniform 40% Fe loading without pore blocking or a substantial reduction in pore size and (2) excellent mass transfer during the FTS reaction. Furthermore, carbon deposition, a principal deactivation mechanism for iron catalysts, can reduce pore size, resulting in diffusional limitations or block pores, causing substantial loss of activity.[25] The high pore volume of the silica-doped alumina apparently accommodates more carbon than conventional alumina, since there is no evidence of activity loss with time. This hypothesis is supported by syngas temperature-programmed-reduction (syngas-TPR) data for the supported catalysts (Figure S2, SI). The observed weight changes under a syngas atmosphere are a combination of several competing reactions: (1) reduction of Fe_2O_3 to lower iron oxides or iron metal, (2) carbiding of iron oxides or iron metal, and (3) carbon deposition (carburization) by the Boudouard reaction ($2CO \rightarrow C + CO_2$). Stages 1 and 2 produce a mass loss; however, stage 3 produces a mass increase due to carbon deposition. The data show a sudden increase in weight (stage 3), indicating that carbon deposition is the dominant reaction above 330 °C, and also show the carburization extent of these catalysts. The extent of carburization for 40Fe/AlSi is about twice that for 40Fe/AlG, indicating that more room is available during reaction for carbon deposition and for reaction.

3. Dehydroxylation of the alumina support to remove acidic sites and hydroxyl groups is very important in FT catalysts. This is facilitated by a high calcination temperature, but that temperature is limited by the γ-Al_2O_3-to-α-Al_2O_3 transition, which usually occurs above 900 °C. During impregnation, adsorbed Fe ions readily react with hydroxyl (OH) groups on the surface of hydroxylated alumina, producing an $FeO{\cdot}Al_2O_3$ surface spinel that cannot be reduced to the active phase under typical reduction/carbiding conditions.[13] Decreasing the OH group content by calcining the support material at high temperatures makes the surface of the alumina more hydrophobic, which decreases the likelihood of further hydroxylation during catalyst preparation and FT reaction in which water is formed.[6,26] Another advantage of removing hydroxyl groups and acidic sites by calcining at high temperatures is to reduce cracking to light hydrocarbons and formation of methane via a formate species.[27] As shown in Figure 4, a dehydroxylation temperature

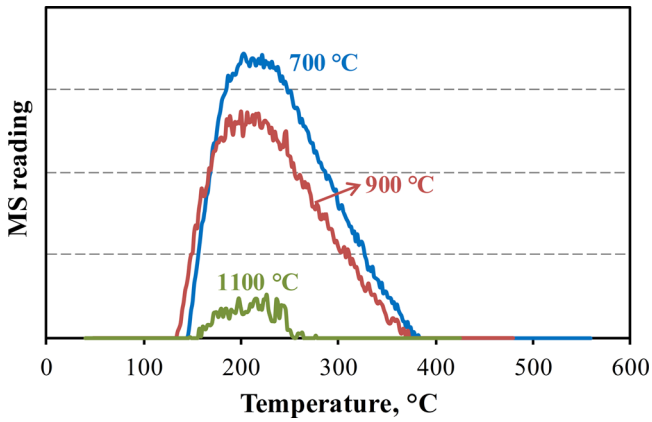

Figure 4. Ammonia-TPD measurements on AlSi calcined at 700, 900, and 1100 °C demonstrating the reduction in acid sites as calcination temperature is increased.

of 1100 °C is very effective in removing most of the acidic sites on AlSi, that is, the acid site concentration is only 48 μmol/g_{cat}, compared with 162 and 236 μmol/g_{cat} on AlSi calcined at 900 and 700 °C, respectively. Although 1100 °C appears to be ideal, the conventional alumina (AlG) support could not be calcined above 700 °C because its surface area and pore volume decrease sharply at higher calcination temperatures as a result of the γ- to α-alumina phase transition.

The greater stability of the AlSi support can be partially explained by examining XRD and solid-state NMR data. From the XRD data in Figure 5 it is observed that the alumina in the AlSi remains γ-alumina up to 1100 °C, theta peaks start to appear at 1200 °C, and alpha peaks appear at 1300 °C. By contrast, Horiuchi et al.[28] observed for their silica-doped alumina that the theta phase appeared at 1100 °C. Further evidence of the amazing stability of our AlSi is indicated by BET surface area and pore volume data taken as a function of temperature (Figure S3,

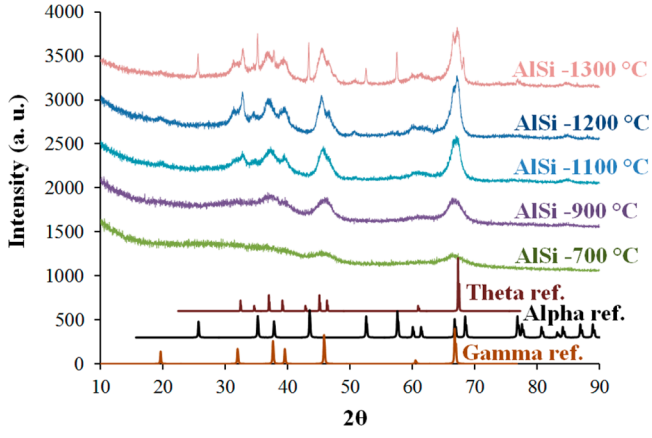

Figure 5. X-ray diffraction patterns of AlSi as a function of temperature, confirming the AlSi support is essentially γ-alumina at 1100 °C.

dx.doi.org/10.1021/cs401242d | ACS Catal. 2014, 4, 1071−1077

SI) that show that AlSi still has a surface area of 110 m^2/g, even after treatment at 1200 °C. For reference, the typical α-alumina has a surface area of 30 m^2/g.

^{27}Al MAS NMR spectra of pure alumina and 5% silica-doped alumina (AlSi) samples show peaks at $\delta \sim +15$, 40, and 75 ppm (Figure 6A,). These peaks are assigned to aluminum in octahedral, tetrahedral, and five-coordinated environments, respectively.[29,30] These results show that the percent of tetrahedral Al in alumina with 0% silica and 5% silica is constant (Figure 6A). We believe that aluminum in tetrahedral sites is not replaced by silicon, as reported by Horiuchi et al.,[31] but rather, Si enters the tetrahedral vacancies in the defect spinel structure of alumina and forms a Si−Al spinel phase. Alumina with silica wt % < 28 forms a Si−Al spinel structure.[32] ^{29}Si MAS NMR (Figure 6B) also shows a peak from −81 to 89 ppm that is attributed to $Si(OAl)_4$ and $Si(OAl)_3OH$. No peak is observed at −110 ppm, which is assigned to the separate SiO_4 phase, confirming that silicon ions form a Si−Al spinel phase and retard the alpha-to-gamma transition. This suggests why AlSi maintains its structure to significantly higher temperatures than conventional γ-aluminas.

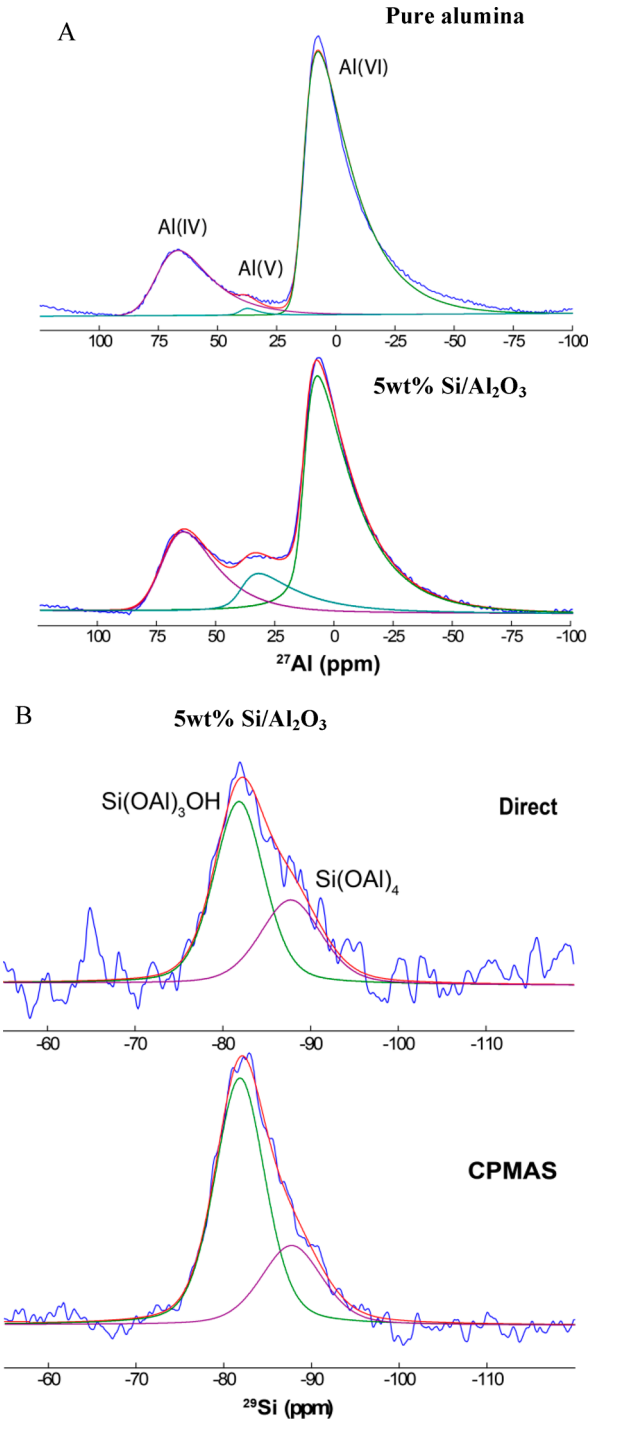

Figure 6. (A) ^{27}Al MAS NMR for pure alumina and 5 wt % BYU silica-doped alumina (AlSi). (B) ^{29}Si MAS NMR and ^{29}Si CPMAS for 5 wt % BYU silica-doped alumina (AlSi).

4. Stabilization of Fe phases against sintering. That catalyst activity continues to increase up to 700 h (29 days) is unprecedented and indicates that sintering of the Fe carbide does not occur on this time-scale. By comparison, sintering of Co catalysts under commercially relevant operation has been observed within a period of just 10 days.[33] On the basis of previous literature, one might hypothesize that SiO_x species on the surface of alumina could be anchoring the iron particles to the alumina surface, thereby preventing crystallite or atomic migration, which apparently occurs during FTS on Co.[34] According to the syngas-TPR results, carburization of 40Fe/AlSi was incomplete, even up to 350 °C, as only a 16.2% weight loss was observed compared with the theoretical weight loss of 24% for reduction of Fe_2O_3 to iron carbide. Thus, 40Fe/AlSi is possibly still being carbided after 700 h, and the activity increases as more active carbide sites are formed. Unreduced iron may also impede surface diffusion of carbon and iron atoms that would lead to sintering. In addition, AlSi has particle sizes <5 nm, on the basis of XRD peak-broadening calculations using the Scherrer formula[35] and TEM (SI Figure S4). Therefore, given the small particle size and high surface area of AlSi, we suggest that the Si−Al spinel structure is mostly available on the surface, which consequently helps anchor the active phase to the support and prevent sintering.

CONCLUSIONS

In summary, the results of this work demonstrate for the first time the preparation of a supported Fe catalyst of high activity and excellent stability for Fischer−Tropsch synthesis. This was made possible by four important attributes: (1) the use of a nonaqueous, slurry impregnation technique for catalyst preparation; (2) the use of a high pore volume, large pore diameter, and stable support, which facilitates a high Fe loading while still maintaining good mass transfer for the FTS reaction; (3) the addition of silica to the support, which adds thermal stability by suppressing the phase transformation of γ-Al_2O_3 to α-Al_2O_3, thus enabling effective dehydroxylation of the alumina surface at high temperatures; and (4) anchoring the active phase to the alumina surface by SiO_x species, thus preventing sintering.

ASSOCIATED CONTENT

Supporting Information

XRD scans of the reduced and carbided catalysts (Figure S1), syngas-TPR profiles (Figure S2), BET properties of AlSi as a function of temperature (Figure S3), TEM and XPS of AlSi (Figures S4, S5), BET property comparisons (Table S1), crystallite sizes from XRD (Table S2), and catalytic data and its comparison with supported and unsupported Fe catalysts from the literature (Tables S3−S5). This material is available free of charge via the Internet at http://pubs.acs.org.

dx.doi.org/10.1021/cs401242d | ACS Catal. 2014, 4, 1071−1077

AUTHOR INFORMATION

Corresponding Author

*E-mail: hecker@byu.edu.

Notes

The authors declare no competing financial interest.

ACKNOWLEDGMENTS

The financial support for this work was provided by members of the Brigham Young University Fischer−Tropsch Consortium and the University of Wyoming Clean Coal Technologies program. Appreciation is expressed to Michael Albretson, Dane Bennion, Brad Chandler, Phillip Childs, Logan Clark, Grant Harper, Jonathon Horton, and McCallin Fisher of the Brigham Young University Catalysis Group for technical assistance in this work. The solid state NMR was performed at Sandia National Laboratories (TMA) which is a multi-program laboratory managed and operated by Sandia Corporation, a wholly owned subsidiary of Lockheed Martin Corporation, for the U.S. Department of Energy's National Nuclear Security Administration under contract DE-AC04-94AL85000.

REFERENCES

(1) (a) Bukur, D. B.; Koranne, M.; Lang, X.; Rao, K. R. P. M.; Huffman, G. P. *Appl. Catal., A* **1995**, *126* (1), 85−113. (b) Bukur, D. B.; Lang, X.; Ding, Y. *Appl. Catal., A* **1999**, *186* (1,2), 255−275. (c) Bukur, D. B.; Lang, X.; Mukesh, D.; Zimmerman, W. H.; Rosynek, M. P.; Li, C. *Ind. Eng. Chem. Res.* **1990**, *29* (8), 1588−1599. (d) Bukur, D. B.; Lang, X. *Ind. Eng. Chem. Res.* **1999**, *38* (9), 3270−3275.

(2) Bukur, D. B.; Sivaraj, C. *Appl. Catal., A* **2002**, *231* (1−2), 201−214.

(3) (a) Wan, H.-J.; Wu, B.-S.; An, X.; Li, T.-Z.; Tao, Z.-C.; Xiang, H.-W.; Li, Y.-W. *J. Nat. Gas Chem.* **2007**, *16*, 130−138. (b) Yang, Y.; Xiang, H.; Zhang, R.; Zhong, B.; Li, Y. *Catal. Today* **2005**, *106*, 170−175. (c) Yang, Y.; Xiang, H.-W.; Tian, L.; Wang, H.; Zhang, C.-H.; Tao, Z.-C.; Xu, Y.-Y.; Zhong, B.; Li, Y.-W. *Appl. Catal., A* **2005**, *284*, 105−122.

(4) O'Brien, R. J.; Xu, L.; Bao, S.; Raje, A.; Davis, B. H. *Appl. Catal., A* **2000**, *196* (2), 173−178.

(5) O'Brien, R. J.; Xu, L.; Spicer, R. L.; Davis, B. H. *Energy Fuels* **1996**, *10*, 921−926.

(6) Xu, J.; Bartholomew, C. H.; Sudweeks, J.; Eggett, D. L. *Top. Catal.* **2003**, *26* (1−4), 55−71.

(7) Rameswaran, M.; Bartholomew, C. H. *J. Catal.* **1989**, *117*, 218.

(8) (a) Torres Galvis, H. M.; Bitter, J. H.; Khare, C. B.; Ruitenbeek, M.; Dugulan, A. I.; de Jong, K. P. *Science (Washington, DC, U. S.)* **2012**, *335* (6070), 835−838. (b) Torres Galvis, H. M.; Bitter, J. H.; Davidian, T.; Ruitenbeek, M.; Dugulan, A. I.; de Jong, K. P. *J. Am. Chem. Soc.* **2012**, *134* (39), 16207−16215.

(9) (a) Karimi, A.; Nasernejad, B.; Rashidi, A. M.; Tavasoli, A.; Pourkhalil, M. *Fuel* **2014**, *117*, 1045−1051. (b) Tavasoli, A.; Trépanier, M.; Abbaslou, R. M. M.; Dalai, A. K.; Abatzoglou, N. *Fuel Process. Technol.* **2009**, *90* (12), 1486−1494. (c) Bahome, M. C.; Jewell, L. L.; Hildebrandt, D.; Glasser, D.; Coville, N. J. *Appl. Catal., A* **2005**, *287*, 60−67. (d) van Steen, E.; Prinsloo, F. F. *Catal. Today* **2002**, *71* (3−4), 327−334. (e) Chen, W.; Fan, Z.; Pan, X.; Bao, X. *J. Am. Chem. Soc.* **2008**, *130*, 9414−9419.

(10) (a) Bartholomew, C. H.; Woodfield, B. F.; Huang, B.; Olsen, R. E.; Astle, L. Method for making highly porous, stable metal oxide with a controlled pore structure. U.S. Patent 2011-US29472, 20110322, 2011. (b) Mardkhe, M. K.; Woodfield, B. F.; Bartholomew, C. H. A method of producing thermally stable and high surface area Al_2O_3 catalyst supports. U.S. Patent 61-851-506, 2013.

(11) Cook, K. M. *Understanding Noble Metal Addition in Cobalt Fischer−Tropsch Catalysts*; Ph.D. Thesis, Brigham Young University, Provo, UT, 2012.

(12) Liu, S.; Liu, Q.; Boerio-Goates, J.; Woodfield, B. F. *J. Adv. Mater.* **2007**, *6*, 18−23.

(13) Dumesic, J. A.; Topsøe, H. *Adv. Catal.* **1977**, *26*, 121−246.

(14) Huang, B.; Bartholomew, C. H.; Woodfield, B. F. *Microporous Mesoporous Mater.* **2014**, *184*, 112−121.

(15) Chu, C.; Hamidy, M.; Nobe, K. *J. Chem. Eng. Data* **1971**, *16*, 327−331.

(16) Massiot, D.; Fayon, F.; Capron, M.; King, I.; Calvé, S. L.; Alonso, B.; Durand, J. O.; Bujoli, B.; Gan, Z.; Hoatson, G. *Magn. Reson. Chem.* **2002**, *40*, 70−76.

(17) Brunner, K. M. *Novel iron catalyst and Fixed-Bed reactor model for the Fischer−Tropsch synthesis*; Ph.D. Thesis, Brigham Young University, Provo, UT, 2012.

(18) Jean-Marie, A.; Griboval-Constant, A.; Khodakov, A. Y.; Diehl, F. *C. R. Chim.* **2009**, *12* (6−7), 660−667.

(19) Yang, C.; Zhao, H.; Hou, Y.; Ma, D. *J. Am. Chem. Soc.* **2012**, *134*, 15814−15821.

(20) Ma, W.; Jacobs, G.; Graham, U. M.; Davis, B. H. *Top. Catal.* **2013**, DOI: 10.1007/s11244-013-0212-1.

(21) Ma, W.; Ding, Y.; Vazquez, V. H. C.; Bukur, D. *App. Catal., A* **2004**, *268*, 99−106.

(22) Kuo, J. C. W. *Two Stage Process for Conversion of Synthesis Gas to High Quality Transportation Fuels*; Mobil Research and Developement Corp.: Paulsboro, N.J., 1985.

(23) Li, S.; Krishnamoorthy, S.; Li, A.; Meitzner, G. D.; Iglesia, E. *J. Cat.* **2002**, *206*, 202−217.

(24) Naidoo, P. The Development and commercialization of a supported cobalt Fischer−Tropsch synthesis Catalyst for the Sasol Gas-to-Liquids Process. In *Autumn School*; Sasol Technology R&D: Cape Town, South Africa, 2012.

(25) Bartholomew, C. H. *Appl. Catal., A* **2001**, *212* (1−2), 17−60.

(26) Fang, H.; Gao, J. F.; Wang, H. T.; Chen, C. S. *J. Membr. Sci.* **2012**, *403−404*, 41−46.

(27) Lee, W. H.; Bartholomew, C. H. *J. Catal.* **1989**, *120*, 256−271.

(28) Horiuchi, T.; Chen, L.; Osaki, T.; Sugiyama, T.; Suzuki, K.; Mori, T. *Catal. Lett.* **1999**, *58* (2,3), 89−92.

(29) Stone, W. E. E.; El Shafei, G. M. S.; Sanz, J.; Selim, S. A. *J. Phys. Chem.* **1993**, *97* (39), 10127−32.

(30) Chen, F. R.; Davis, J. G.; Fripiat, J. J. *J. Catal.* **1992**, *133* (2), 263−278.

(31) Heemeier, M.; Frank, M.; Libuda, J.; Wolter, K.; Kuhlenbeck, H.; Bäumer, M.; Freund, H.-J. *Catal. Lett.* **2000**, *68*, 19−24.

(32) Chakraborty, A. K. *Adv. Appl. Ceram.* **2006**, *105* (6), 297−303.

(33) (a) Tsakoumis, N. E.; Rønning, M.; Borg, Ø.; Rytter, E.; Holmen, A. *Catal. Today* **2010**, *154*, 162−182. (b) Saib, A. M.; Moodley, D. J.; Ciobîcă, I. M.; Hauman, M. M.; Sigwebela, B. H.; Weststrate, C. J.; Niemantsverdriet, J. W.; van de Loosdrecht, J. *Catal. Today* **2009**, *154* (3−4), 271−282.

(34) de Tymowski, B.; Liu, Y.; Meny, C.; Lefevre, C.; Begin, D.; Nguyen, P.; Pham, C.; Edouard, D.; Luck, F.; Pham-Huu, C. *App. Catal., A* **2012**, *419−420*, 31−40.

(35) Patterson, A. L. *Phys. Rev.* **1939**, *56*, 978−82.

NOTE ADDED AFTER ASAP PUBLICATION

After this paper was published ASAP on March 3, 2014, additional information was added to the Acknowledgments. The corrected version was reposted March 5, 2014.